NASA Contractor Report 191115

Thermomechanical Fatigue Damage/Failure Mechanisms in SCS-6/Timetal 21S $[0/90]_s$ Composite

Michael G. Castelli
NYMA, Inc.
Engineering Services Division
Brook Park, Ohio

June 1994

Prepared for
Lewis Research Center
Under Contract NAS3–27186

National Aeronautics and
Space Administration

Trade names or manufacturers' names are used in this report for identification only. This usage does not constitute an official endorsement, either expressed or implied, by the National Aeronautics and Space Administration.

Thermomechanical Fatigue Damage/Failure Mechanisms in SCS-6/Timetal 21S $[0/90]_s$ Composite

Michael G. Castelli
NYMA, Inc.
Engineering Services Division
2001 Aerospace Parkway
Brook Park, Ohio 44142

ABSTRACT

The thermomechanical fatigue (TMF) deformation, damage, and life behaviors of SCS-6/Timetal 21S $[0/90]_s$ were investigated under zero-tension conditions. In-phase (IP) and out-of-phase (OP) loadings were investigated with a temperature cycle from 150 to 650°C. An advanced TMF test technique was used to mechanically quantify damage progression. The technique incorporated explicit measurements of the macroscopic *i*) isothermal static moduli at the temperature extremes of the TMF cycle and *ii*) coefficient of thermal expansion (CTE) as functions of the TMF cycles. The importance of thermal property degradation and its relevance to accurate post-test data analysis and interpretation is briefly addressed. Extensive fractography and metallography were conducted on specimens from failed and interrupted tests to characterize the extent of damage at the microstructure level. Fatigue life results indicated trends analogous to those established for similar unidirectional [0] reinforced titanium matrix composite systems. High stress IP and mid to low stress OP loading conditions were life-limiting in comparison to maximum temperature isothermal conditions. Dominant damage mechanisms changed with cycle type. Damage resulting from IP TMF conditions produced measurable decreases in static moduli but only minimal changes in the CTE. Metallography on interrupted and failed specimens revealed extensive [0] fiber cracking with sparse matrix damage. No surface initiated matrix cracks were present. Comparable OP TMF conditions initiated environment enhanced surface cracking and matrix cracking initiated at [90] fiber/matrix (F/M) interfaces. Notable static moduli and CTE degradations were measured. Fractography and metallography revealed that the transverse cracks originating from the surface and [90] F/M interfaces tended to converge and coalesce at the [0] fibers.

INTRODUCTION

Titanium matrix composites (TMCs) are currently being developed and evaluated for use in a number of elevated temperature airframe and propulsion system applications. The obvious attraction of such materials is their relatively high strength/low density characteristics when compared to monolithic materials. Though the attractions and potential benefits of TMCs are evident in unidirectional systems with uniaxial loading in the fiber direction, they become much less pronounced with the introduction of off-axis fibers and/or the introduction of loads not coinciding with a primary fiber direction, see Larsen et al., (1993). It is apparent that many of the structural applications for which TMCs are being considered will experience a variety of multiaxial loads, thus, necessitating load carrying capabilities in more than one direction. Therefore, many potential components will incorporate multiple fiber orientations, employing such laminates as the [0/90] and [0/±45/90].

Previous elevated temperature experimental studies of various TMCs containing off-axis fibers have revealed that the tensile (Lerch and Saltsman, 1993; Majumdar and Newaz, 1992), isothermal fatigue (Castelli, 1994a; Gayda and Gabb, 1992; Mall and Portner, 1992; Pollock and Johnson, 1992), and thermomechanical fatigue (TMF) (Castelli and Gayda, 1993; Majumdar and Newaz, 1991; Mall et al., 1992; Mirdamadi and Johnson, 1992; Neu and Nicholas, 1993; Russ and Hanson, 1993) properties are drastically reduced from those exhibited by unidirectional [0] TMCs. Much of this degradation has been attributed to the weak bond at the fiber/matrix (F/M) interface, which appears to either fail at extremely low stresses, or is essentially non-existent beyond that which is mechanically induced by the internal residual stress state. Thus, upon initial loading, marked internal damage is immediately introduced (i.e., F/M de-bonding). In addition, environmental degradation is enhanced by the exposed [90] fiber ends (Castelli; 1994a; 1993a; Gayda and Gabb, 1992), as the SiC fibers serve to pipe oxygen along the F/M interfaces; this condition is likely, for example, in applications where a TMC component contains holes for mechanical fastening. Further, initial experimental studies on clad [0] TMC coupons (where an external titanium layer completely encases a TMC core with no external points of fiber exposure) (Castelli and Gayda, 1993) suggest that many of the environmental concerns remain, given the relatively high oxygen diffusivity rates of titanium alloys.

With the given complexities and concerns for this class of materials, it is essential that the fundamental fatigue damage/failure mechanisms are carefully characterized to guide the theoretical tools being developed to predict their mechanical behaviors under diverse loading conditions. With this specific goal in mind, this study was undertaken to accurately characterize the deformation, damage progression, and fatigue life behaviors of a $[0/90]_s$ TMC under TMF loading conditions. This was accomplished by combining information gathered from three different sources: *i*) the deformation responses, *ii*) optical and scanning electron microscopy (SEM) fractography and metallography (on both failed specimens and those taken from tests interrupted prior to failure), and *iii)* a specialized TMF test technique (Castelli, 1993b) which allows explicit isothermal stiffness (E) and coefficient of thermal expansion (CTE) measurements, tracking macroscopic property degradations. Through the combination and corroboration of these sources, the dominant fatigue damage/failure mechanisms and their relative progressions were characterized.

MATERIAL AND TEST DETAILS

The TMC used in this study was SCS-6/Timetal[1] 21S $[0/90]_s$ with the fiber orientation designation indicating that the external most fibers were in the loading direction (i.e., the [0] orientation). SCS-6 is a SiC fiber with a nominal diameter of 140 μm. Timetal 21S is a metastable ß-titanium alloy with a nominal composition of Ti-15Mo-3Nb-3Al-0.2Si (wt. %). The TMC panel was fabricated by hot isostatic pressing alternate layers of Timetal 21S foil and SCS-6 fiber mat; TiNb ribbon was used as crossweave material in the fiber mats. The composite had a nominal fiber volume ratio of 39% and a nominal thickness of 0.85 mm. Coupon test specimens were cut from the panel using abrasive waterjet machining with no additional edge preparation. All specimens were subjected to a pre-test heat treatment, consisting of an 8 hour soak in vacuum at 621°C, to stabilize the ß+α microstructure of the

[1]Timetal 21S is a registered trademark of TIMET, Titanium Metals Corporation.

Timetal 21S. The coupon specimen design [ref. 15] is a "dogbone" geometry featuring an overall length of 15.2 cm, a radius cut of 37 cm, and a central parallel-sided section of 2.6 cm. This design proved to be very successful at ensuring specimen failures within the controlled section. Tabs were attached to the specimen with adhesive for assembly purposes, and held in position by high clamping forces during the test.

All thermomechanical fatigue tests were conducted in air on a computer-controlled servo-hydraulic test system equipped with water-cooled grips. The tests were load-controlled, zero-tension ($R_\sigma = 0$) with triangular waveforms for both load and temperature commands. In-phase (IP) and out-of-phase (OP) loadings were examined with a cyclic frequency of 5.56×10^{-3} Hz and a temperature cycle of 150 to 650°C; IP and OP TMF conditions were defined as 0° and 180°, respectively, time phase shifts between the load and temperature waveforms. Axial strain measurements were made over a centrally located 12.7 mm gage length with a water-cooled extensometer mounted on the edge of the specimen. Intrinsic K-type thermocouples were used for temperature monitoring and closed-loop control. The thermocouple spot-weld locations did not exhibit premature cracking, and thus were considered to have had minimal influence on the specimen's fatigue life. Specimen failure was defined as complete fracture of the specimen.

The TMF test technique used in this study (Castelli, 1993b) to quantify both the stiffness and the CTE degradations during TMF testing is shown graphically in Fig. 1. After each TMF cycle designated for data collection, the specimen was subjected to a thermal cycle under zero load, represented by the horizontal line from T_1 to T_2 at zero load. This thermal cycle allowed the real-time or "current" thermal strain (ε^{th}) properties of the composite to be explicitly measured with the high temperature extensometer. At the extremes of the thermal cycle (i.e., 150 and 650°C), the temperatures were briefly stabilized and small "elastic" loads were applied; these loadings are represented by the stress-strain lines in Fig. 1 with slopes marked E_1 and E_2. This allowed explicit measurement of the "current" isothermal material stiffness at both temperature extremes. Note that the E measurements are essentially a Young's modulus measurement (see ASTM Standard E 111), except that a proportional limit is not easily identified in this TMC, particularly at elevated temperatures. However, the maximum stress levels used to obtain E were kept relatively small (80 MPa) to facilitate a linear-elastic response.

It is important to emphasize that the material stiffness is defined here as the slope of the initial stress-strain response initiated from zero macroscopic load at an isothermal temperature. As measured, these stiffness values (also referred to as moduli) may differ from those which can be estimated at comparable temperature points along the TMF deformation loops. For example, during an IP TMF test, the E_{650} value as measured by the technique discussed, will likely differ from the tangent modulus at 650°C taken from the deformation loop, which occurs at the maximum cyclic stress. These two measurements potentially represent vastly different states of [90] F/M interface separations, crack openings, constituent stresses, and temperature gradients over the gage section (static versus dynamic), all of which strongly impact the slope of the stress-mechanical strain response, that is, the static[2] "stiffness" measurement. All this is in addition to the assumptions associated with estimating

[2]The term "static" is used here to differentiate between a stiffness value which is measured dynamically, i.e., a so-called dynamic modulus.

an "isothermal" measurement under the dynamic temperature conditions of a TMF cycle. Consequently, the static stiffness values are dependent upon the convention used to make the measurement, and must be interpreted appropriately. The convention employed here was felt to represent the most explicit and informative approach.

Several benefits were realized from this test technique. First, the "real-time" ε^{th} information was essential for an accurate post-test assessment of the mechanical strain (ε^{m}) response; this fact will become evident after viewing the CTE degradation data and discussing the mechanical deformation behavior. Second, the CTE and isothermal E measurements provide a definitive quantitative measurement for tracking the TMF damage progression. Third, measurement of the isothermal E values enables direct stiffness degradation/damage comparisons between TMF and isothermal fatigue loadings.

In comparison to an uninterrupted "conventional" TMF test, this technique introduced several additional thermal cycles at zero load and several relatively small elastic loads. These additional loadings were found to be inconsequential with respect to the ongoing material damage and resulting TMF life. This was verified throughout the development and implementation of the test technique (Castelli, 1993b).

LIFE AND DEFORMATION

Cyclic lives determined under TMF conditions for SCS-6/Timetal 21S $[0/90]_s$ are plotted in Fig. 2. Also shown in this plot are isothermal lives at 650°C for this identical TMC system (cyclic test frequency was $1.0x10^{-2}$ Hz), taken from Castelli, (1994a). In general, cyclic lives determined under TMF conditions were greatly reduced from those obtained under T_{max} (i.e., 650°C) isothermal conditions. Note that the IP and OP life trends cross at a maximum stress (S_{max}) of ≈ 550 MPa, above which the IP conditions are life-limiting and below which OP conditions are more damaging. Also note that at stresses below the IP/OP crossover, IP conditions result in cyclic lives comparable to those experienced under T_{max} isothermal conditions. These TMF life trends are very similar to those exhibited by [0] unidirectional TMCs (Castelli et al., 1992, Gabb et al., 1993, Russ et al., 1991), suggesting potential similarities between the damage mechanisms associated with the cycle types.

A representative deformation response during IP cycling with S_{max} = 500 MPa is shown in Fig. 3. Note that the strains given are ε^{m} and not total strains (ε^{t}), that is, the ε^{th} component is factored out based on the true real-time ε^{th} (subsequently discussed). Selected progressive cycles from the first to slightly before failure are shown to reveal several aspects of the deformation behaviors, including individual cycle hysteresis and overall stiffness with their progressive changes, and the cumulative strain ratchetting. As evidenced from this plot, IP zero-tension TMF loadings introduced conditions which were highly conducive to strain ratchetting. At equivalent S_{max} levels, this behavior was amplified over that found under T_{max} isothermal conditions because of the increasing stiffness on the unload (due to the decreasing temperature) which likely tended to minimize the degree of stress reversal in the matrix. Some degree of stiffness degradation is apparent in Fig. 3; however, a quantitative assessment is complicated not only by the dynamic temperature conditions and strain ratchetting, but also by the various states of F/M de-bonding, crack opening, and other factors (discussed earlier) dictating the instantaneous slope at points along the stress-strain response. Previous room temperature (Johnson et al., 1990; Lerch et al., 1991) and elevated temperature isothermal (Castelli, 1994a; Mall and Portner, 1992; Pollock and Johnson, 1992) studies on similar [0/90]

TMCs have shown that the deformation response typically exhibits a distinct "knee" at the point of assumed [90] F/M interface failure (A "knee" implies a distinct point at which the material compliance markedly increases.). However, this feature was not obvious in cycle 1 of the TMF response and was likely hidden because of the continually changing stiffness resulting from the dynamic temperature conditions. Past research on this TMC system (Castelli, 1994a) suggests that the knee should occur at approximately 150 MPa, where the temperature is approximately 300°C.

In contrast to IP and isothermal loadings, OP loadings did not promote excessive strain ratchetting, as OP maximum loading occurred at T_{min} where matrix load shedding and tensile strain ratchetting was less likely to occur. In similar fashion to Fig. 3, a representative OP deformation response is shown in Fig. 4 where the S_{max} value was 300 MPa; these conditions yielded a cyclic life comparable to the S_{max} = 500 MPa IP test shown in Fig. 3. In general, only minor increases in minimum ε^m occurred throughout the OP tests indicating the lack of strain ratchetting. The maximum ε^m values, however, typically revealed clear increases, indicating decreases in the overall "TMF stiffness". This behavior is characteristically illustrated in Fig. 4 (quantitative values discussed subsequently). A note of caution is warranted when qualitatively interpreting this Fig., as the mechanical strain scale is quite different from Fig. 3, given the relatively small strains incurred during OP TMF tests. Note also that the loops exhibited a distinct convex curvature toward the right; this was promoted by the dynamically increasing stiffness with load and temperature, overriding the decreasing tangential stiffness trend which is normally associated with increasing load. As was the case for the IP deformation, no distinct knee was apparent in the stress-strain response.

DAMAGE/FAILURE MECHANISMS

The dominant damage/failure mechanisms present in SCS-6/Timetal 21S $[0/90]_s$ varied as a functions of cycle type. As suggested by the trends established in the fatigue life plot, many of the mechanisms were similar to those found in [0] TMCs (Castelli et al., 1992). However, additional damage mechanisms were introduced by including fibers transverse to the loading direction, most notably, cracking initiated at the [90] F/M interfaces. The physical damage in the microstructure will be discussed initially, as this information will add insight to the interpretation of the macroscopic property degradation curves.

Fractography and Metallography

For comparison purposes, metallographic observations made from isothermal testing at 650°C on this $[0/90]_s$ TMC (Castelli, 1994a) will be briefly summarized. Fracture surfaces from all stress levels revealed environment assisted internal matrix cracking. Oxidation patterns on the fracture surfaces and extensive metallography indicated that the matrix cracks were initiated at [90] F/M interfaces and propagated normal to the loading in the specimen thickness direction. Based on the extent of internal oxidation it was evident that the [90] fibers served to pipe oxygen along the F/M interfaces enhancing internal environment assisted cracking. Surface initiated matrix cracking could not be identified at any of the stress levels investigated. Metallographic mounts revealed that all [90] F/M interfaces were de-bonded. Longitudinal sections taken from [0] fiber plies revealed little or no [0] fiber cracking or de-bonding with one exception; localized de-bonding and enhanced oxidation occurred at the TiNb crossweave ribbon. In general, a single dominant damage mode was revealed: environment assisted matrix cracking initiated exclusively at the [90] F/M interfaces.

Fracture surfaces taken from IP TMF specimens revealed distinct and unique features relative to those found under isothermal and OP conditions. All IP fracture surfaces exhibited ductile matrix failure over the entire cross-section as typically shown by the SEM fractography in Fig. 5. Matrix in contact with the [90] fibers revealed a relative increase in oxidation (based on discoloration), again confirming the oxygen "piping" effect noted under isothermal conditions. However, fatigue cracking initiated at the [90] F/M interfaces was not evident on the fracture surfaces. A relative increase in [0] fiber pullout was also visible. In general, all IP features closely resembled those produced by monotonic tensile failures, a trend which was also noted in [0] TMCs (Castelli et al., 1992)

Comprehensive metallography on failed specimens revealed global de-bonding of the [90] fibers in the loading direction. Limited matrix cracks, predominantly transverse to the loading direction, were found to initiate at [90] F/M interfaces, but their relative size and number were greatly reduced from those produced under comparable isothermal and OP conditions. SEM of the specimens' surfaces revealed no surface cracking confirming the fractographic observations. Clearly, the dominant damage present under IP conditions was extensive [0] fiber cracking, as shown in Fig. 6 by the longitudinal section exposing a [0] fiber ply. The majority of fibers appeared to be broken into lengths of 200 to 400 μm, suggesting a relationship to a characteristic load development length. Close inspections at high magnifications revealed that the cracks typically stopped (or began) at the interfaces of the outer carbon/carbon coating of the SCS-6 fibers and did not reach (or start at) the interfaces of the reaction zone/carbon coating. In these cases, the bond between the reaction zone and the outer carbon coating of the SCS-6 fiber appeared to be intact. Note, however, that the exact initiation points of the fiber cracks are unclear because the fibers were always found to be cracked across their full diameter. As was found under isothermal conditions, localized [0] fiber de-bonding and enhanced oxidation at the TiNb crossweave intersections were visible; however, these appeared to have no influence on [0] fiber cracking.

Metallography on IP test specimens interrupted prior to failure revealed that the [0] fiber cracking occurred relatively early in cyclic life. Under IP TMF conditions with S_{max} = 500 MPa, [0] fiber cracking was visible at the earliest interrupted value of 200 cycles, that is, $\approx$ 20% N_f. This observation is consistent with a study by Neu and Roman, (1993), where TMF damage in a unidirectional TMC was monitored through acoustic emissions. Their work indicated that a number of [0] fiber fractures occurred within the first 2 cycles of an IP test where $N_f > 4000$ cycles.

OP TMF conditions introduced a mechanism not present under 650°C isothermal or IP TMF loadings, namely, surface initiated fatigue cracking. Fracture characteristics and oxidation patterns strongly suggested crack initiation points at both surface and [90] F/M interface locations. Oxidized cracks initiated at the surface appeared to propagate transversely (i.e., through the thickness) in toward the [0] fibers, and oxidized cracks initiated at the [90] F/M interfaces propagated transversely out toward the [0] fibers. Upon failure, a "strip" of matrix exhibiting ductile failure characteristics was created along the centerline of the [0] fibers. This failure mode is shown in Fig. 7. Note the foil/foil interface at the center of the ductile strip; this defines what is referred to as the "centerline" of the [0] fiber. These ductile strips were most notable under high and mid S_{max} levels. Under relatively low S_{max} conditions, surface initiated and [90] F/M interface initiated cracks were able to meet at the [0] fibers prior to overload failure, exhibiting fatigue fracture surfaces which were cracked through the entire thickness.

SEM of OP specimen surfaces and thorough metallography confirmed the fracture surfaces' indications. Extensive surface cracking transverse to the loading direction, such as that shown in Fig. 8, was evident over the entire gage section for all OP conditions. In general, the number of visible surface cracks increased with increasing S_{max}; however, relatively low S_{max} conditions tended to produce cracks exhibiting a more torturous path with increased crack branching. By longitudinally sectioning into the thickness of the specimen, it was evident that cracks were propagating both in from the surface and out from the [90] fibers. This is exhibited in Fig. 9 where several secondary cracks are shown that had not yet propagated through the entire thickness. The majority of [90] fibers exhibited multiple crack initiations. Close examination of these secondary cracks revealed apparent initiation points at both the *i*) interfaces of the outer carbon/carbon coatings of the SCS-6 fibers, and *ii*) interfaces of the reaction zone/carbon coating. As previously observed under IP conditions, all [90] fibers exhibited some degree of de-bonding in the loading direction. Sections exposing the [0] ply revealed a complete absence of [0] fiber cracking. The only damage associated with the [0] fiber was localized de-bonding and enhanced oxidation coinciding with the TiNb crossweave, as found in isothermal and IP tests. However, this appeared to have no influence on the matrix cracking.

Metallography on OP test specimens interrupted prior to failure revealed that both surface and [90] F/M interface initiated cracks occurred extremely early in cyclic life. A specimen interrupted as early as 7% of the expected cyclic life (i.e., N = 100 with an expected N_f = 1394) revealed several small surface cracks and multiple [90] F/M interface initiated cracks. All of the [90] fibers exhibited F/M de-bonding in the loading direction, as this likely occurs on the first cycle.

Stiffness Degradation

Shown in Fig. 10 are the isothermal moduli (E) measurements collected for the two TMF experiments whose deformation behaviors were previously discussed (Figs. 3 and 4). These two stress levels were again selected to show stiffness degradations under IP and OP conditions resulting in comparable TMF lives. Each TMF test is represented by two curves consisting of the isothermal E values measured at the temperature extremes of the TMF cycles, i.e., E_{150} and E_{650}. Also shown in this plot are the E_{650} values taken from an isothermal test at 650°C with an S_{max} value of 500 MPa. Several key observations can be made concerning the damage progression.

First, it was obvious that the damage accumulation, in terms of stiffness degradation, changed with cycle type. This is reasonable given that observations from the fractography and metallography indicated distinct differences. Under IP TMF conditions with S_{max} = 500 MPa, first cycle degradation was evident (a 6% drop), and quantitatively very similar to those found under 650°C isothermal fatigue conditions (shown) and OP TMF conditions (not shown) with S_{max} = 500 MPa. For all tests conducted on this material, the degree of initial stiffness degradation was more closely related to S_{max} rather than cycle type, and in general, was found to increase with increasing S_{max}. It is likely that this initial stiffness degradation is strongly associated with the [90] F/M de-bonding. As stated earlier, one advantage of this test technique was that it allows for direct quantitative comparisons between isothermal and TMF damage based on stiffness degradation. By comparing the S_{max} = 500 MPa IP TMF and 650°C isothermal tests, one notes that although the lives are not dramatically different (see Fig. 2) and the first-cycle E_{650} degradations are essentially identical, the damage progression is

notably different. Prior to failure, the isothermal specimen experienced a 13% degradation in E_{650}, whereas the comparable IP TMF specimen experienced a 26% drop in this same property. This, in spite of the fact that the environmental degradation was likely heightened in the isothermal case where the material was loaded at 650°C for a test duration of 43 hours, in comparison to the IP TMF specimen which experienced continuous cycling from 150 to 650°C for 54 hours (This statement is corroborated by a qualitative assessment of the relative oxidations of the specimen surfaces and fracture surfaces.). This highlights the enhanced damage progression introduced by the synergistic effects associated with TMF conditions.

Fig. 10 also indicates that the IP loading condition promoted similar degradation behaviors in the E_{150} and E_{650} values, as represented by the fairly constant gap between the two dashed lines. The data suggest that the ongoing composite damage is impacting the "low" temperature stiffness in much the same way as it is impacting the "high" temperature stiffness. Recall from above that the dominant progressive damage under IP conditions was [0] fiber cracking associated with a lesser degree of matrix damage at the de-bonded [90] interfaces. Also note that the stiffness of the SCS-6 fiber is relatively insensitive to temperature over this temperature range (Textron Specialty Materials). If the broken [0] fiber segments are sufficiently small and/or sufficient de-bonding occurs along the damaged [0] fibers, in turn compromising the load transfer, the effective contribution of the fiber stiffness to the composite stiffness will be degraded. Such a reduction of the effective fiber contribution to the composite stiffness will promote quantitatively comparable reductions at 150 and 650°C. This, essentially, is the trend established by the IP damage progression, quantitatively characterized in Fig. 10.

In contrast to the IP behavior, the E values measured from the OP specimen did not degrade equally, but rather, the E_{150} or "low" temperature E values degraded more severely. This trend was most evident under mid to low S_{max} values where the progression of matrix cracking through the cross-section was sufficiently "mature" prior to the effective overload failure. For the OP test presented in Fig. 10 (i.e., S_{max} = 300 MPa), the composite E values at both temperature extremes were essentially equal just prior to failure where the material is in a highly damaged state. Qualitative information from the fractography and metallography discussed above indicated that environment enhanced matrix fatigue cracking was the primary damage mechanism, with little or no [0] fiber cracking. Considering again a straightforward interpretation of the composite stiffness based on constituent contributions, one notes that the matrix contribution is much greater at 150°C than at 650°C. This comes from the fact that the stiffness of the Timetal 21S matrix (unlike the SCS-6 fiber) is strongly dependent upon temperature in this temperature range (Castelli et al., 1994). Given this, and considering a continual degradation of the effective matrix stiffness in the absence of [0] fiber cracking, the relative degradation of the composite $E_{150°C}$ values will be greater than that experienced by the composite $E_{650°C}$ values. Further, in the extreme case where the matrix is "completely" damaged and contributes nothing to the composite stiffness, the composite E values at both temperature extremes will be essentially equal, given that the SCS-6 fiber stiffness is relatively insensitive to temperature over this temperature range. In agreement with the microstructural observations, this appears to be the progression of damage quantitatively characterized by the data given in Fig. 10.

Coefficient of Thermal Expansion Degradation

Degradations of the mean CTEs are shown in Fig. 11 for the IP and OP tests discussed in Fig. 10. The mean CTE was calculated by taking the ε^{th} range from 150 to 650°C and dividing it by ΔT, that is, 500°C. Thus, it represents the average CTE for the TMF temperature cycle. In general, damage resulting from IP TMF loadings produced a relatively small decrease in the mean CTE early in cyclic life. However, this property appeared to stabilize and remain essentially constant throughout the cyclic life of the specimen. Although a significant degree of stiffness degradation was taking place as a likely result of [90] F/M de-bonding and damage associated with [0] fiber cracking, it appears that the impact of this type of damage on the macroscopic CTE is minimal.

In contrast, cyclic damage resulting from OP TMF conditions appeared to have a notable effect on the composite CTE. Degradation of this macroscopic property was again most pronounced and severe under mid to low S_{max} values (i.e., conditions which resulted in relatively long lives). Fig. 11 illustrates that under OP conditions with S_{max} = 300 MPa, this property experienced a degradation of 22%. The extensive matrix damage in the presence of undamaged [0] fibers allowed the composite mean CTE to tend towards the lower CTE dictated by the [0] fibers. The magnitude of degradation will of course be strongly influenced by the relative percentage of [0] fibers and the remaining transverse stiffness imposed by the [90] fibers. It is apparent that under loading conditions which promote extensive matrix cracking, measurement of the CTE degradation provides a straightforward quantitative means for tracking the progression of composite damage. This was also found to be the case for similar [0] (Castelli, 1994b) and [90] (Castelli, 1993a) unidirectional TMCs subjected to TMF loadings. This type of information should also be extremely useful for the verification of analytical damage modeling for this class of materials.

As a related issue, it is important to point out the significance of CTE degradation with respect to interpreting the deformation behavior. The data conclusively show that it is erroneous to assume that the thermal strain component remains constant throughout the course of the test (as is commonly done in the literature to date). This macroscopic property of the TMC is more accurately interpreted as a "structural" response, rather than an elastic property, given that it is a function of the constituents and laminate orientations, and clearly changes with damage state (Castelli, 1993a; 1993b; Hashin, 1990; 1988), inelasticity, and internal stress state (Urquhart et al., 1993). Consequently, if the various load-controlled test data (isothermal and TMF) are to be accurately represented in terms of "mechanical strain" (i.e., $\varepsilon^t - \varepsilon^{th}$) the current ε^{th} must be known. Also, without tracking the true ε^{th}, techniques used to estimate TMC stiffness from the TMF deformation response (either qualitatively or quantitatively) will likely be in error, and in some cases, significantly so. Further, in load-controlled testing (such as that presented above), ignorance of the true ε^{th} will only lead to data reduction errors. In contrast, in strain-controlled testing, ignorance of the true ε^{th} can lead to test-control errors introducing unknown shifts in the mean ε^m under isothermal conditions, and unknown changes in both the mean and range of ε^m under TMF conditions; see Castelli, (1993b) for further discussion.

SUMMARY

An experimental investigation was conducted to characterize the deformation, damage, and cyclic life of SCS-6/Timetal 21S $[0/90]_s$ under thermomechanical fatigue (TMF) loading conditions. In-phase and out-of-phase cycles were investigated with a temperature cycle of

150 to 650°C under load-controlled, zero-tension conditions. The progression of TMF damage was quantified through the use of a unique TMF test procedure which allowed measurements of the composite isothermal static moduli and coefficient of thermal expansion (CTE) during the TMF tests. By comparing the 1) deformation behaviors, 2) observations made from fractography and metallography, and 3) degradations of the composite mechanical properties, a lucid characterization of the damage/failure mechanisms was obtained. These mechanisms were found to strongly depend upon cycle type, and clearly point to the need for a mechanistic approach to damage modeling in titanium matrix composites. The following summarizes the major findings of this work:

150-650°C In-Phase TMF

- IP loadings promoted the most aggressive strain ratchetting, and of the cycle types discussed, were life-limiting at high cyclic stress levels.
- Static moduli degradations were evident and comparable at both extremes of the temperature cycle.
- CTE degradations were relatively small and appear to occur early in cyclic life.
- The dominant damage was [0] fiber cracking and a to a lesser degree transverse matrix cracking initiated at the de-bonded [90] F/M interfaces.
- De-bonding and environmental degradation was enhanced at TiNb crossweave locations; however, no effect on [0] fiber cracking was apparent.
- No surface initiated cracking was evident.

150-650°C Out-of-Phase TMF

- OP loadings did not promote aggressive strain ratchetting, and of the cycle types discussed, were life-limiting at moderate and low cyclic stress levels.
- Static moduli degradations were evident at both extremes of the temperature cycle; however, the relative degradation was much greater at T_{min}, particularly under mid and low cyclic stress levels (i.e., conditions leading to relatively long cyclic lives).
- Degradation of the composite CTE was evident and found to be most severe under mid to low cyclic stress levels. This property appeared to be a good indicator of matrix damage.
- The dominant damage exhibited two components: *i*) environment enhanced surface initiated cracking, and *ii*) transverse matrix cracking initiated at the de-bonded [90] F/M interfaces.
- De-bonding and environmental degradation was enhanced at TiNb crossweave locations; however, no effect on matrix cracking was apparent.
- Minimal, if any, [0] fiber cracking was found.

ACKNOWLEDGEMENTS

Thanks be to God. The author also wishes to acknowledge Rod Ellis for his support and input to this research and Chris Burke, Ralph Corner, and Ron Shinn for their assistance in the Fatigue and Structures Laboratory and the Metallographic Laboratory at NASA Lewis Research Center.

REFERENCES

Castelli, M.G. (1994a). Isothermal Damage and Fatigue Behavior of SCS-6/Timetal 21S $[0/90]_s$ Composite at 650°C. *Composites*, submitted for publication.

Castelli, M.G. (1994b). Thermomechanical Deformation, Damage and Life of SCS-6/Timetal 21S $[0]_4$. *Int. J. of Fatigue*, submitted for publication.

Castelli, M.G. (1993a). Thermomechanical and Isothermal Fatigue Behavior of a $[90]_8$ Titanium Matrix Composite. *Proc. of The Amer. Soc. for Composites 8th Tech. Conf. on Composite Material, Mechanics, and Processing*, pp. 884-892.

Castelli, M.G. (1993b). An Advanced Test Technique to Quantify Thermomechanical Fatigue Damage Accumulation in Composite Materials. *J. of Composites Tech. and Res.*, to appear; also NASA CR 191147.

Castelli, M.G., Arnold, S.M. and Saleeb, A.F. (1994). Specialized Deformation Tests for the Characterization of a Viscoplastic Model: Application to a Titanium Alloy. NASA TM 106268, National Aeronautics and Space Administration, Washington, D.C.

Castelli, M.G. and Gayda, J. (1993). An Overview of Elevated Temperature Damage Mechanisms and Fatigue Behavior of a Unidirectional SCS-6/Ti-15-3 Composite. DE-Vol. 55, *Reliability, Stress Analysis, and Failure Prevention*, ASME, pp. 213-221.

Castelli, M.G., Bartolotta, P.A. and Ellis, J.R. (1992). Thermomechanical Testing of High-Temperature Composites: Thermomechanical Fatigue Behavior of SiC(SCS-6)/Ti-15-3. *Composite Materials: Testing and Design (Tenth Volume), ASTM STP 1120*, G.C. Grimes, Ed., Philadelphia, pp. 70-86.

Gabb, T.P., Gayda, J., Bartolotta, P.A., and Castelli, M.G. (1993). A Review of Thermomechanical Fatigue Damage Mechanisms in Titanium and Titanium Aluminide Matrix Composites. *Int. J. of Fatigue*, Vol. 15, No. 5, pp. 413-422.

Gayda, J. and Gabb, T.P. (1992). Isothermal Fatigue Behavior of a $[90]_8$ SiC/Ti-15-3 Composite at 426°C. *Int. J. of Fatigue*, Vol. 14, No. 1, pp. 14-20.

Hashin, Z. (1990). "The Effect of Microcracking on Thermal Expansion and Cyclic Stress-Strain Relations of Composites," *Microcracking-Induced Damage in Composites*, American Society of Mechanical Engineering Winter Annual Meeting, AMD Vol. 111, pp. 35-40.

Hashin, Z. (1988). "Thermal Expansion Coefficients of Cracked Laminates," *Composites Science and Technology*, Vol. 31, pp. 247-260.

Johnson, W.S., Lubowinski, S.J. and Highsmith, A. L. (1990). Mechanical Characterization of SCS_6/Ti-15-3 Metal Matrix Composites at Room Temperature. *Thermal and Mechanical Behavior of Ceramic and Metal Matrix Composites, ASTM STP 1080*, J.M. Kennedy, H.H Moeller and W.S. Johnson, Eds., Philadelphia, pp. 451-489.

Larsen, J.M., Russ, S.M. and Jones, J.W. (1993). Possibilities and Pitfalls in Aerospace Applications of Titanium Matrix Composites. *NATO AGARD Conf. on Characterization of Fiber Reinforced Titanium Metal Matrix Composites*, Bordeaux, France, Sept.

Lerch, B.A. and Saltsman, J.F. (1993). Tensile Deformation of SiC/Ti-15-3 Laminates. *Composite Materials: Fatigue and Fracture Fourth Volume, ASTM STP 1156*, W.W. Stinchcomb & N.E. Ashbaugh, Philadelphia, pp. 161-175.

Lerch, B.A., Melis, M.E. and Tong, M. (1991). Experimental and Analytical Analysis of Stress-Strain Behavior in a $[0/90]_{2s}$, SiC/Ti-15-3 Laminate. NASA TM 104470, National Aeronautics and Space Administration, Washington D.C.

Majumdar, B.S. and Newaz, G.M. (1992). Inelastic Deformation of Metal Matrix Composites: Plasticity and Damage Mechanisms - Part II. NASA TM 189096, National Aeronautics and Space Administration, Washington, D.C.

Majumdar, B.S. and Newaz, G.M. (1991). Thermomechanical Fatigue of a Quasi-Isotropic Metal Matrix Composite. *Composite Materials: Fatigue and Fracture (Third Volume), ASTM STP 1110*, T.K. O'Brien, Ed., Philadelphia, pp. 732-752.

Mall, S. and Portner, B. (1992). Characterization of Fatigue Behavior in Cross-Ply Laminate of SCS-6/Ti-15-3 Metal Matrix Composite at Elevated Temperature. *J. of Eng. Mat. and Tech.*, Vol. 114, Oct. pp. 409-415.

Mall, S. Hanson, D.G., Nicholas, T. and Russ, S.M. (1992). Thermomechanical Fatigue Behavior of a Cross-Ply SCS-6/ß21-S Metal Matrix Composite. *Constitutive Behavior of High Temperature Composites*, MD-Vol. 40, B.S. Majumdar, G.M. Newaz and S. Mall, Eds. ASME, pp. 91-106.

Mirdamadi, M. and Johnson, W.S. (1992). Stress-Strain Analysis of a $[0/90]_{2s}$ Titanium Matrix Laminate Subjected to a Generic Hypersonic Flight Profile. NASA TM 107584, National Aeronautics and Space Administration, Washington D.C.

Neu, R.W. and Nicholas, T. (1993). Effect of Laminate Orientation on the Thermomechanical Fatigue Behavior of Titanium Matrix Composites. *J. of Composites Tech. and Res.*, submitted for publication.

Neu, R.W. and Roman, I. (1993). Acoustic Emission Monitoring of Damage in Metal Matrix Composites Subjected to Thermomechanical Fatigue. *Composites Science and Technology*, submitted for publication.

Pollock, W.D. and Johnson, W.S. (1992). Characterization of Unnotched SCS-6/Ti-15-3 Metal Matrix Composites at 650°C. *Composite Materials: Testing and Design (Tenth Volume), ASTM STP 1120*, G.C. Grimes, Ed., Philadelphia (1992) pp. 175-191.

Russ, S.M. and Hanson, D.G. (1993). Fatigue and Thermomechanical Fatigue of a SiC/Titanium $[0/90]_{2s}$ Composite. *Fatigue '93*, Vol. 2, J.P. Bailon and I.J. Dickson, Eds., Eng. Mat. Advisory Services, Ltd., U.K., pp. 1085-1090.

Russ, S.M., Nicholas, T., Bates, M. and Mall, S. (1991). Thermomechanical Fatigue of SiC/Ti-24Al-11Nb Metal Matrix Composites. *Failure Mechanisms in High Temperature Composite Materials*, AD-Vol. 22 and AMD-Vol. 122, Eds. G.K. Haritos, G. Newaz and S. Mall, ASME, New York, pp. 37-43.

Textron Specialty Materials Data Sheet, Silicon Carbide Composite Materials.

Urquhart, E., Arnold, S.M., Pindera, M.J. and Aikin, B.J. (1993). Simulation of Experimentally Observed Thermal Expansion Behavior of FeCrAlY-Based Composites *Advanced High Temperature Engine Materials Technology Program*, NASA CP 19117, Vol. II, Oct., National Aeronautics and Space Administration, Washington D.C., pp. 54:1-12.

Worthem, D.W. (1990). Flat Tensile Specimen Design for Advanced Composites. NASA CR 185261, National Aeronautics and Space Administration, Washington D.C.

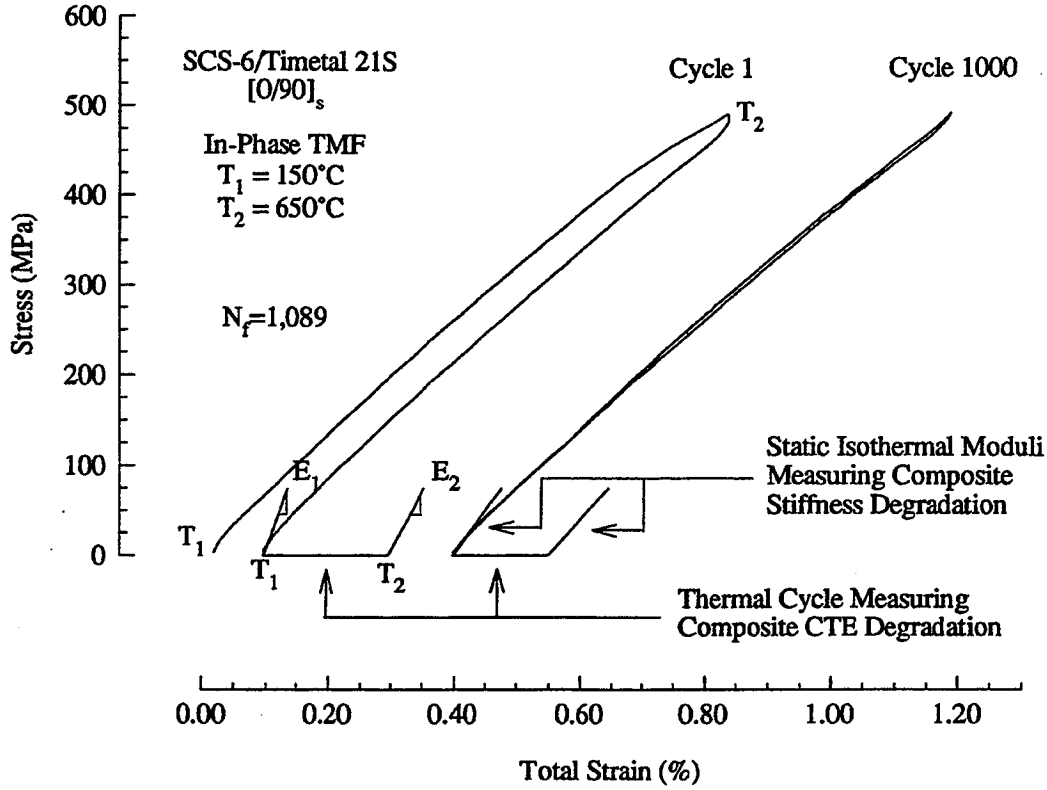

Figure 1.-Advanced test technique to quantify thermomechanical fatigue damage by explicitly measuring isothermal static moduli and coefficient of thermal expansion.

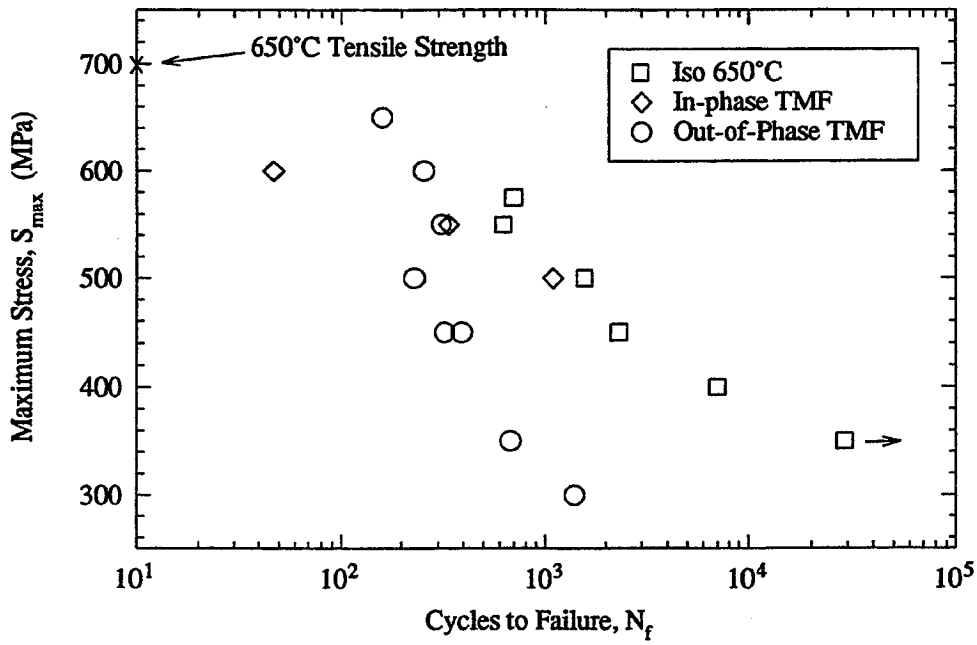

Figure 2. Thermomechanical fatigue life of SCS-6/Timetal 21S $[0/90]_s$ with a temperature cycle of 150-650°C.

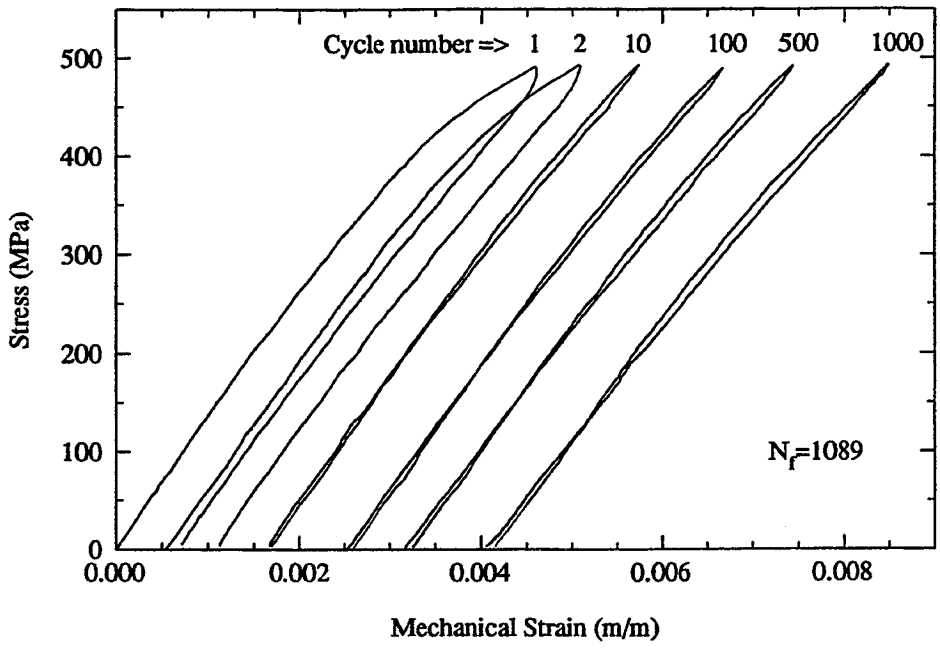

Figure 3. In-phase thermomechanical fatigue deformation of SCS-6/Timetal 21S $[0/90]_s$ with S_{max} = 500 MPa.

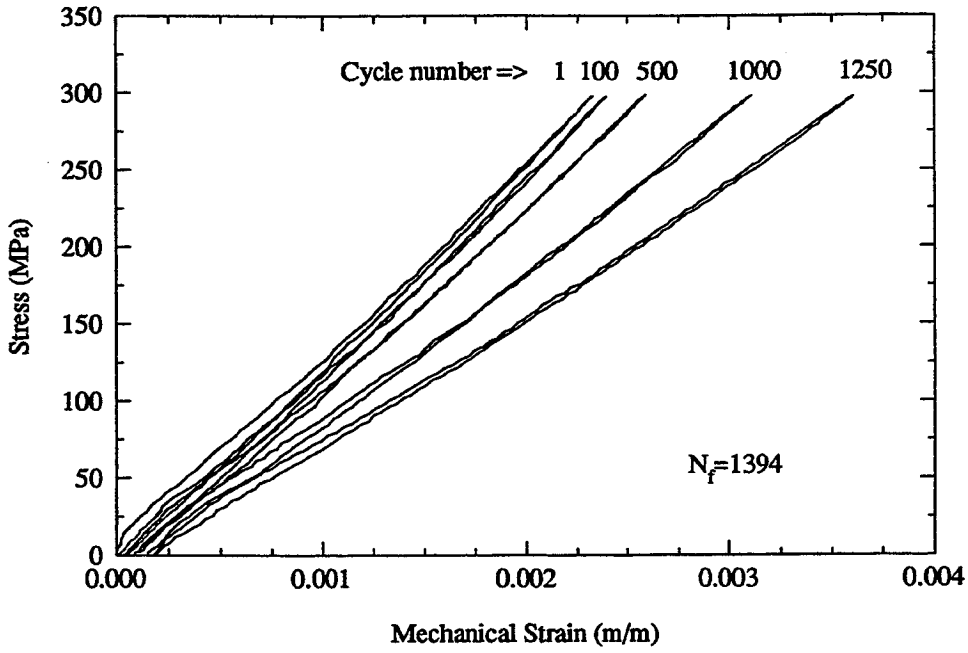

Figure 4. Out-of-phase thermomechanical fatigue deformation of SCS-6/Timetal 21S $[0/90]_s$ with S_{max} = 300 MPa.

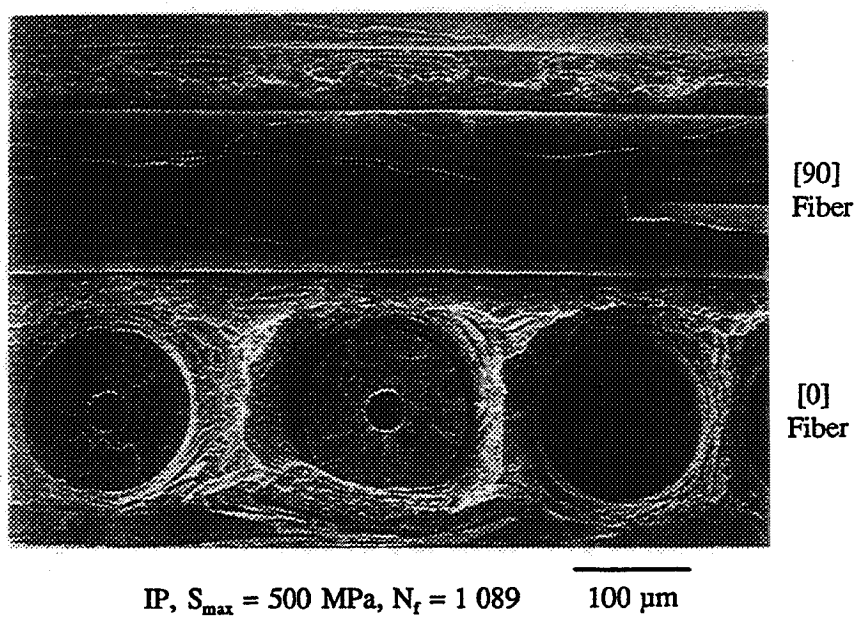

Figure 5. SEM fracture surface highlighting the ductile matrix failure associated with IP TMF loading.

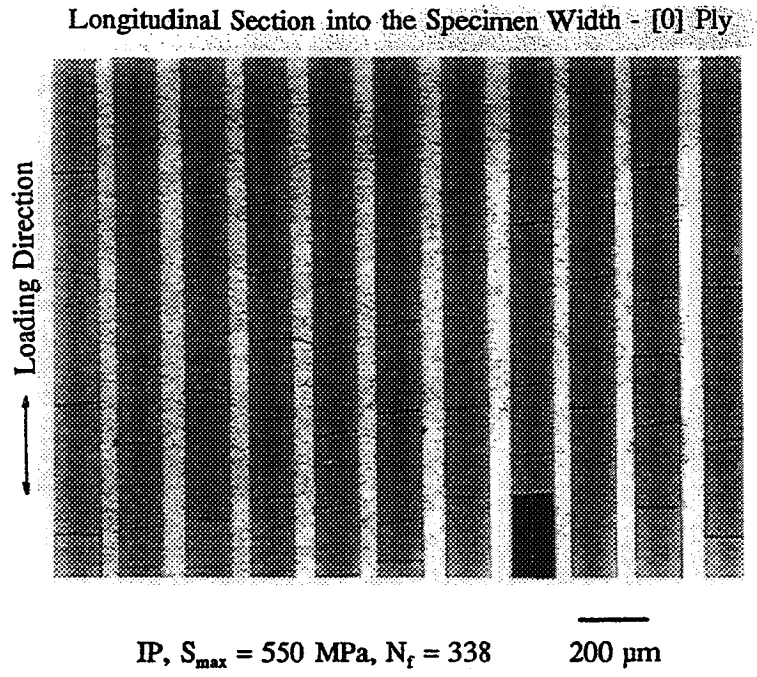

Figure 6. Metallographic section showing extensive [0] fiber cracking associated with IP TMF loadings.

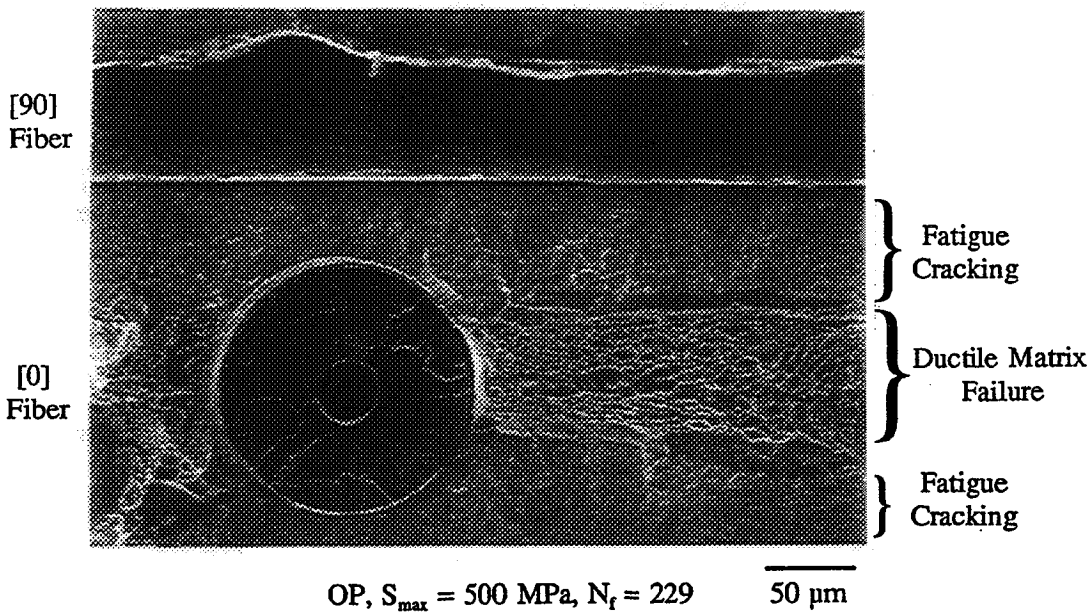

Figure 7. SEM fracture surface showing transverse fatigue cracking in from the surface and out from the [90] F/M interfaces forming a ductile matrix "centerline strip" along the [0] fibers upon failure.

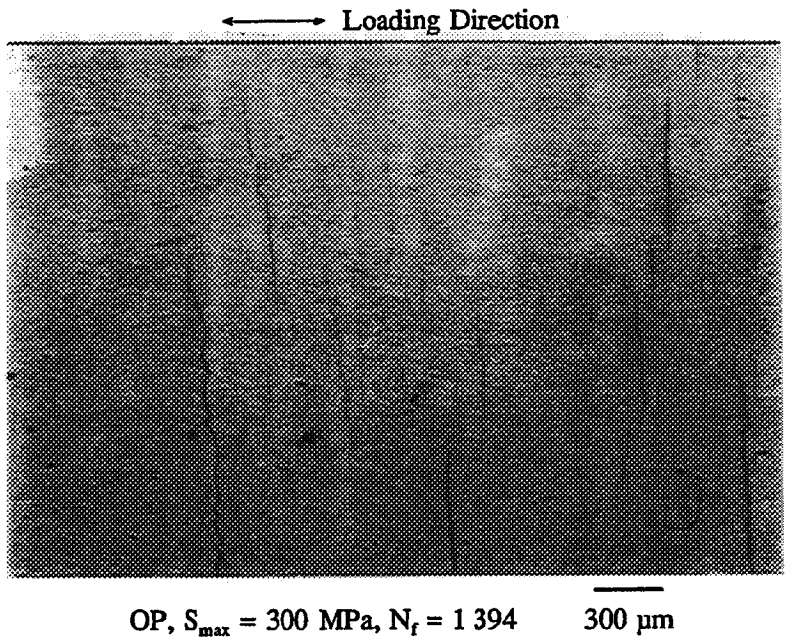

Figure 8. SEM surface picture showing extensive surface cracking associated with OP TMF loadings.

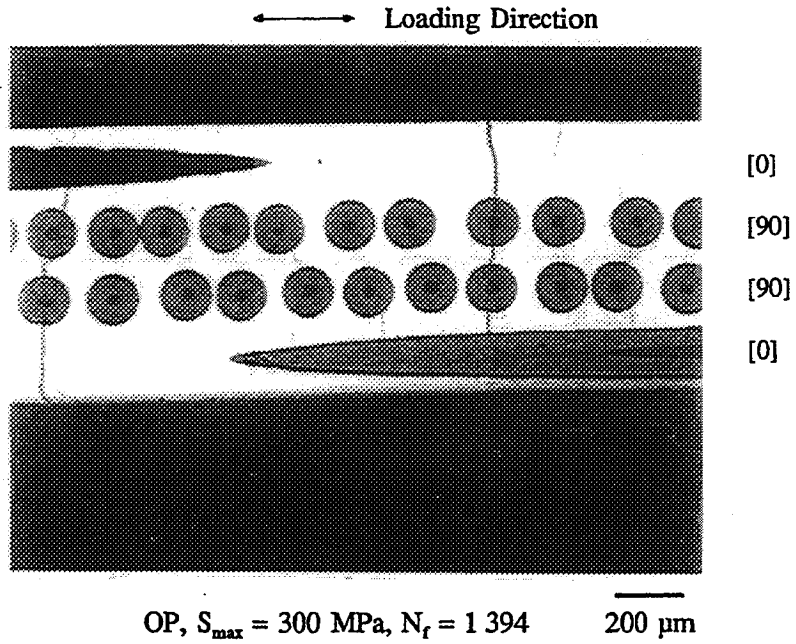

Figure 9. Metallographic section showing matrix cracks initiated at both surface and [90] F/M interface locations.

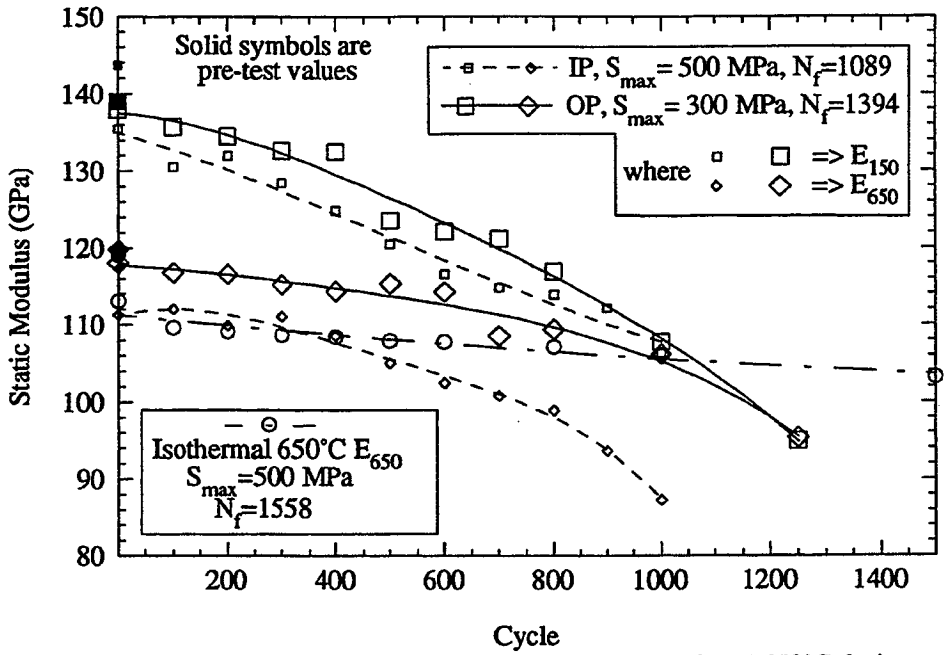

Figure 10. Degradation of the isothermal static moduli at 150 and 650°C during IP and OP thermomechanical fatigue of SCS-6/Timetal 21S $[0/90]_s$.

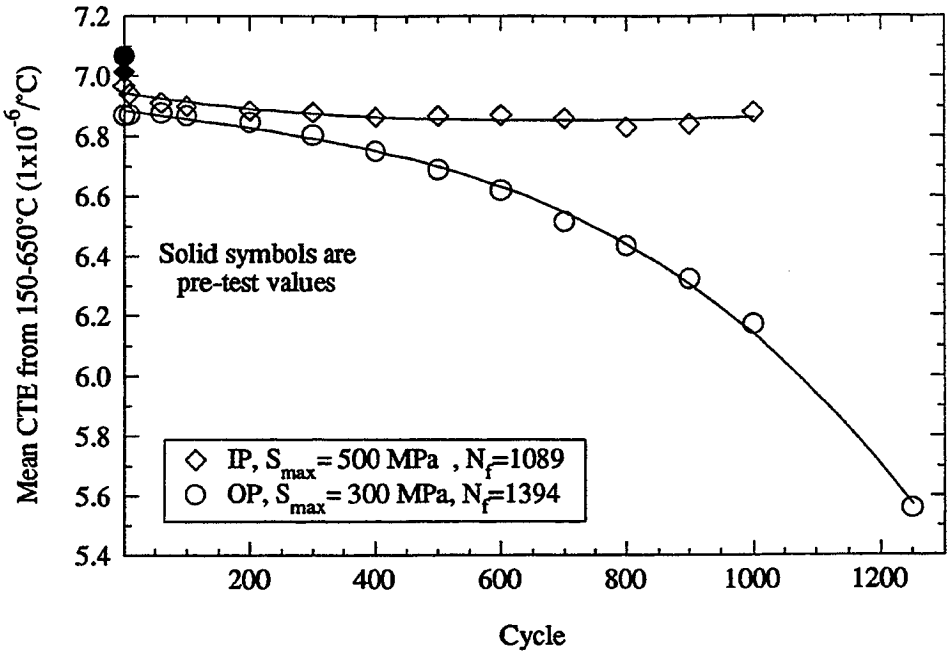

Figure 11. Degradation of the mean coefficient of thermal expansion from 150 to 650°C during IP and OP TMF of SCS-6/Timetal 21S $[0/90]_s$.

REPORT DOCUMENTATION PAGE

Form Approved
OMB No. 0704-0188

1. AGENCY USE ONLY (*Leave blank*)	2. REPORT DATE	3. REPORT TYPE AND DATES COVERED
	June 1994	Final Contractor Report

4. TITLE AND SUBTITLE

Thermomechanical Fatigue Damage/Failure Mechanisms in SCS-6/Timetal 21S $[0/90]_s$ Composite

5. FUNDING NUMBERS

WU–763–22–41
C–NAS3–27186

6. AUTHOR(S)

Michael G. Castelli

7. PERFORMING ORGANIZATION NAME(S) AND ADDRESS(ES)

NYMA, Inc.
Engineering Services Division
2001 Aerospace Parkway
Brook Park, Ohio 44142

8. PERFORMING ORGANIZATION REPORT NUMBER

E–8940

9. SPONSORING/MONITORING AGENCY NAME(S) AND ADDRESS(ES)

National Aeronautics and Space Administration
Lewis Research Center
Cleveland, Ohio 44135–3191

10. SPONSORING/MONITORING AGENCY REPORT NUMBER

NASA CR–191115

11. SUPPLEMENTARY NOTES

Project Manager, Rod Ellis, Structures Division, NASA Lewis Research Center, organization code 5220, (216) 433–3340.

12a. DISTRIBUTION/AVAILABILITY STATEMENT

Unclassified - Unlimited
Subject Category 24

12b. DISTRIBUTION CODE

13. ABSTRACT ***(Maximum 200 words)***

The thermomechanical fatigue (TMF) deformation, damage, and life behaviors of SCS-6/Timetal 21S $[0/90]_s$ were investigated under zero-tension conditions. In-phase (IP) and out-of-phase (OP) loadings were investigated with a temperature cycle from 150 to 650°C. An advanced TMF test technique was used to mechanically quantify damage progression. The technique incorporated explicit measurements of the macroscopic *i*) isothermal static moduli at the temperature extremes of the TMF cycle and *ii*) coefficient of thermal expansion (CTE) as functions of the TMF cycles. The importance of thermal property degradation and its relevance to accurate post-test data analysis and interpretation is briefly addressed. Extensive fractography and metallography were conducted on specimens from failed and interrupted tests to characterize the extent of damage at the microstructure level. Fatigue life results indicated trends analogous to those established for similar unidirectional [0] reinforced titanium matrix composite systems. High stress IP and mid to low stress OP loading conditions were life-limiting in comparison to maximum temperature isothermal conditions. Dominant damage mechanisms changed with cycle type. Damage resulting from IP TMF conditions produced measurable decreases in static moduli but only minimal changes in the CTE. Metallography on interrupted and failed specimens revealed extensive [0] fiber cracking with sparse matrix damage. No surface initiated matrix cracks were present. Comparable OP TMF conditions initiated environment enhanced surface cracking and matrix cracking initiated at [90] fiber/matrix (F/M) interfaces. Notable static moduli and CTE degradations were measured. Fractography and metallography revealed that the transverse cracks originating from the surface and [90] F/M interfaces tended to converge and coalesce at the [0] fibers.

14. SUBJECT TERMS

Titanium matrix composites; Thermomechanical fatigue; Damage mechanisms; Stiffness loss; CTE; Metallography

15. NUMBER OF PAGES
20

16. PRICE CODE
A03

17. SECURITY CLASSIFICATION OF REPORT	18. SECURITY CLASSIFICATION OF THIS PAGE	19. SECURITY CLASSIFICATION OF ABSTRACT	20. LIMITATION OF ABSTRACT
Unclassified	Unclassified	Unclassified	